A bio-impedance analysis method (BIAM) based on human hand anatomy for hand gesture recognition

Haofeng Chen[1,2],Gang Ma[1,2],Peng Wang[2,3] and Xiaojie Wang[1,2,3]

***Abstract*—In this paper, we presented a bio-impedance analysis method (BIAM) based on human hand anatomy, and propose a feasible and flexible BIAM system to obtain the bio-impedance signals for different gestures to achieve a high classification accuracy in hand gesture recognition with flexibility in electrode arrangement and fewer electrodes. To verify the proposed method, 11 gestures including two sets: hand gestures and pinch gestures were selected for the experiment. Based on the functional structure of the human hand, we identified appropriate electrode positions and placed five electrodes on the hand surface for bio-impedance signal measurement. Compared to the electrical impedance tomography (EIT) method, which uses a band with the same number of electrodes wrapped around the wrist, the proposed method achieved 98.7% recognition accuracies on the hand gesture set and 97.8% on the pinch gesture set, while the EIT can only achieved 97.1%, and 86.3%, respectively. In particular the proposed method demonstrated the advantage of distinguishing gestures with similar muscle contractions.**

***Index Terms*—bio-impedance , electrodes, hand gesture recognition , electrical impedance tomography , measurements.**

I. Introduction

HAND gesture based human-computer-interaction (HCI) plays an important role in human life. Capturing the intention of hand movement allows for the control of robotic arms or hand prostheses to complete specific tasks such as handling harmful substances, moving heavy objects, and operating a remote surgery [1]. Obtaining and interpreting the signals, that contain reliable information related to hand motion, is crucial for hand gesture recognition. The image signal of hand motion captured by a camera referred to as machine vision technology is commonly used to recognize hand position and pose [2]–[4]. Although the image signal provides rich information about gestures, it is sensitive to the external environment (line-of-sight, color, light). Vision based gesture recognition will not work for cases where the objects are outside the scope of the camera. An alternative approach is to detect the on-body signals using contact sensors. Measureable on-body signals can be divided into non-biological and biological signals. Non-biological signals related to the hand gesture recognition are mostly involved in force, pressure, and acceleration measurements. For example, the force-sensing resistor (FSR) sensors were attached to a user's wrist for gesture recognition by monitoring the change in resistance with respect to the muscular activities [5], [6]. An air-pressure sensor was proposed to recognize the muscle contraction of the wrist by measuring the change of the air pressure in an air bladder contacting the muscles of interest [7]. This method converts the muscle movement displacement of the wrist into a measurable force or pressure to realize gesture recognition. The accelerometers and gyroscopes were applied to capture the intention of hand movement by measuring the inertial force [8], [9] for dynamic hand gesture recognition. However, it is not suitable for static gesture recognition owing to its low sensitivity to low-speed motion. All non-biological signal approaches are heavily dependent on the physical movement of the muscles and bones in the hands and arms. When the muscle movement is less distinguishable, it leads to a poor recognition rate or even failure. Biological signals corresponding to the physiological activities of human beings provide fine details of the intention of hand movement. Surface electromyography (sEMG) is the most commonly used method for biological signal acquisition. The electric impulses produced by skeletal muscles are acquired through electrodes attached to the skin of the wrist and arm, and can be decoded for hand gesture recognition [10]. However, the sEMG signal was very weak and sensitive to electric noise. Additionally, the raw sEMG signals are noisy where filter circuits and complex preprocessing are needed [11], [12], which makes the sEMG system bulky, and increases the computational costs. An alternative biological signal sensing method for hand gesture recognition is based on the electrical impedance tomography (EIT) technique, which detects and decodes the changes in muscular bio-impedance. Zhang and Harrison [13] were the first to design an EIT system with two-pole measurement scheme to classify eight hand gestures in real time by reconstructing the cross-sectional impedance of the wrist. Later, they upgraded the EIT system by using more electrodes and a more sophisticated "four-pole" scheme to achieve a mean accuracy of 94.3% with 32 electrodes on 11 gestures [14]. Wu et al. [1] found the limitation of the hardware design in [13], [14] and presented a high-performance EIT system using commercial ICs, which achieved an accuracy of 98% for gesture recognition in controlling hand prosthesis motion. Yao et al. [15] investigated the effects of electrode shapes and materials on the performance of a wearable EIT system for hand gesture recognition. They found that an

*This work was supported by the Fundamental Research Funds for the Central Universities under Grants WK5290000001, the Open Funding Project of National Key Laboratory of Human Factors Engineering, Grant NO.6142222190311 and Anhui ProvincialNatural Science Foundation, Grant No.1908085MF196.

[1]Institute of Intelligent Machines, Hefei Institute of Physical science, Chinese Academy of Sciences, Hefei 230031, China

[2]Department of Precision Machinery and Precision Instrumentation, University of Science and Technology of China, Hefei, Anhui 230026, China

[3]Engineering Research Center of Automotive Electronics and Embedded System, Chongqing University of Posts and Telecommunications, Chongqing 400065, China

Corresponding author:xjwang@iamt.ac.cn

increase in the contact impedance between the electrode and skin could improve the accuracy of recognition. However, it is still questionable how to obtain stable and distinguishable contact impedances at the wrist to recognize finer gestures such as thumb-to-finger gestures for different users. Most of EIT gesture recognition systems employ two-dimensional (2D) EIT electrode arrangements to map the internal impedance distribution onto a cross-sectional plane of a wrist. Recently, Jiang et al. [16] proposed a three-dimensional (3D) EIT system to improve the accuracy of hand gesture recognition. They distributed 16 electrodes equally on two wristbands, one wrapped around the wrist and the other wrapped further up the forearm for 3D EIT measurement. It appears that a great number of the electrodes and appropriate electrode positions can effectively improve the distinguishability of impedance measurements. In a previous study [17], we optimized the EIT drive pattern based on feature selection and model explanation to reduce the number of electrodes and achieve a performance trade-off between the accuracy and time response for real-time gesture recognition. Hyvonen et al. [18] proposed a methodology based on a Bayesian approach to optimize the electrode positions for improving the quality of EIT reconstructions. Smyl et al. [19] proposed a straightforward deep-learning based approach to optimize the electrode positions in EIT sensing. All these approaches serves the purpose of the reconstruction of an unknown impedance distribution. Because gesture recognition as a classification problem only requires a subset of the original impedance data for classification rather than tomography, reconstruction of the internal impedance distribution of a wrist is not necessary. On the one hand, the cross section of the human wrist has an irregular shape and it would be difficult to reconstruct the impedance distribution for different users. On the other hand, the electrodes on the wrist might move with contraction of the wrist muscles, which might lead to unreliable reconstruction results. In this paper, inspired by the EIT technology, we propose a bio-impedance analysis method (BIAM) based on human hand anatomy to detect the minimum change in bio-impedance of the human body corresponding to the hand movement. This method can obtain considerable information to achieve high classification accuracy in hand gesture recognition with flexibility in electrode arrangement and fewer electrodes. To validate the proposed method, we designed a four-wire–two-terminal BIAM sensing system. Eleven gestures mentioned in [13], [17] including two sets: hand gestures and pinch gestures were selected in the tests. Based on the functional structure of the human hand, we identified appropriate electrode positions and placed five electrodes on the hand surface for bio-impedance signal measurement. The measured impedance values obtained from the five electrodes formed a ten-dimensional impedance feature. For comparison, the same five electrodes were evenly attached to the wrist, which is commonly used in EIT hand gesture recognition. The separability criterion based on the distances of between-class and within-class [20] was used to evaluate the two given impedance feature sets: one captured by BIAM and the other obtained by EIT.

II. Measurement of Hand Muscular Activity by Bio-Impedance Sensing

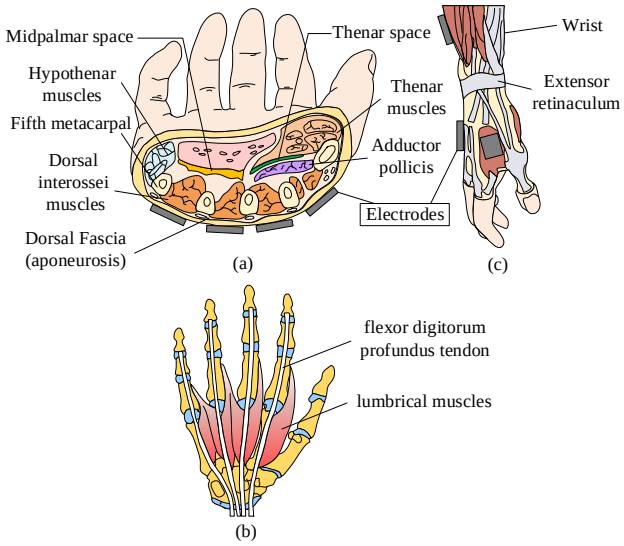

Fig. 1. Electrode placement based on human hand anatomy model. (a) Transverse section through the middle of the palm illustrating the fascial compartments of the hand. (b) Lumbricals distribution (Palmar views). (c).Lateral view of deep layer of extensor muscles [21].

In this section, we analyzed the muscular activities according to the human hand anatomy model, and attempted to find the optimal electrode positions for bio-impedance measurement. As shown in Fig.1(a), the intrinsic muscles of the hand can be divided into four parts: thenar muscles, adductor pollicis, hypothenar muscles, short muscles of the hand. The thenar muscles are located in the thenar compartment and contains abductor pollicis brevis, flexor pollicis brevis, and opponens pollicis, which are chiefly responsible for opposition of the thumb. The adductor pollicis is located in the adductor compartment of the hand, and functions to adduct the thumb and move the thumb to the palm of the hand. The hypothenar muscles produce hypothenar eminence on the medial side of the palm and move the little finger. The short muscles of the hand are the lumbricals and interossei. As shown in Fig. 1(b), there are four slender lumbrical muscles attached to the four fingers outside the thumb, and the starting point is attached to the flexor digitorum profundus tendon. The lumbricals flex the fingers at the metacarpophalangeal joints and extend the interphalangeal joints [21]. Among all intrinsic muscles of the hand The dorsal interosseous muscles are the most dorsally located. The four dorsal interosseous muscles (dorsal interossei) are located between the five metacarpals and are mainly responsible for abducting fingers. With the help of these hand muscles, the hand can make a variety of gestures. The movement of these muscles directly reflects the movement of the hand, and the movement of these muscles is more obvious than that of the wrist. Four electrodes were placed near the dorsal muscles to capture the relative movement between the fingers, and one electrode on the dorsal wrist to capture wrist movement, as shown in Figure 1(c). Fig.2 (a-g) show the relative change in the electrode position caused by hand movement in accordance with the six hand gestures.

We established a Cartesian coordinate system with the center of the electrode at the wrist as the origin. Taking fist and relax gestures as examples, in the vertical plane, the angle between the line connecting the electrode at the wrist and the electrode at the back of the hand and the coordinate axis is α. When creating a fist, α is positive. When relaxing, α is negative. We can see that the five electrode positions cause the electrode displacement to change significantly for different hand gestures, resulting in a distinguishable bio-impedance change.

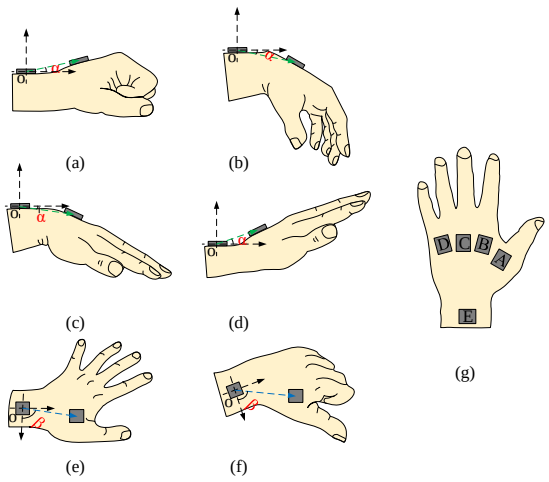

Fig. 2. The relative change of electrode position between different gestures. (a) Fist (b) Relax (c) Right (d) Left (e) Stretch (f) Thumbs up (g) the position of the five electrodes on the hand.

For BIAM gesture recognition, the detected bio-impedance signals directly account for classification accuracy. The measured impedance Z_m includes three components.

$$\mathrm{Z}_m = Z_{\sigma_{hand}} + Z_{contact} + \varepsilon_{noise} \tag{1}$$

where $Z_{\sigma_{hand}}$ is the bio-impedance across the tissues and bones inside the hand, $Z_{contact}$ is the contact impedance between the electrode and body skin, and ε_{noise} is the measurement error from the hardware system and the environmental noise. The measured impedance values obtained from the five electrodes form a ten-dimensional impedance feature, which is used to distinguish the class of gestures.

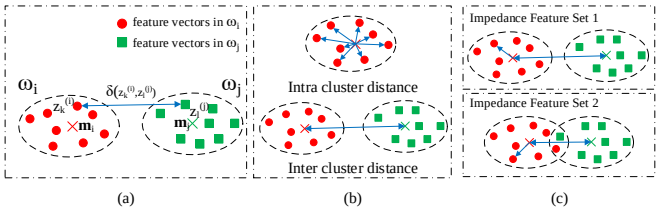

Fig. 3. The separability criterion. (a) the distance between two vectors. (b) intra class distance and inter class distance. (c) the separability of two feature sets.

To improve the accuracy of gesture recognition, we should reduce the contact impedance as well as the system measurement error, and enhance the discrimination of internal impedance signals by optimizing the electrode positions. In other words, we should increase the impedance feature separability of all classes of gestures as much as possible. The separability criterion [20] is typically used to evaluate the class separability. As shown in Fig. 3 (a), $\mathbf{z}_k^{(i)}, \mathbf{z}_l^{(j)}$ are the L-dimensional feature vectors in class ω_i and ω_j , respectively, and $\delta(\mathbf{z}_k^{(i)}, \mathbf{z}_l^{(j)})$ is the distance between these two vectors, then the average distance between various feature vectors is expressed as follows.

$$J_d(\mathbf{z}) = \frac{1}{2}\sum_{i=1}^{M} P_i \sum_{j=1}^{M} P_j \frac{1}{n_i n_j} \sum_{k=1}^{n_i}\sum_{l=1}^{n_j} \delta(\mathbf{z}_k^{(i)}, \mathbf{z}_l^{(j)}) \tag{2}$$

where M is the number of classes, n_i is the number of samples in class ω_i , n_j is the number of samples in class ω_j , P_i and P_j are the prior probabilities of the corresponding classes. We use Euclidean distance to represent the distance between two vectors, and thus we obtain:

$$\delta(\mathbf{z}_k^{(i)}, \mathbf{z}_l^{(j)}) = (\mathbf{z}_k^{(i)} - \mathbf{z}_l^{(j)})^T(\mathbf{z}_k^{(i)} - \mathbf{z}_l^{(j)}) \tag{3}$$

Using $\mathbf{m}_i$ to represent the mean vector of the i-th sample set, and $\mathbf{m}$ to represent the total average vector of all types of sample sets, we obtain:

$$\mathbf{m}_i = \frac{1}{n_i}\sum_{k=1}^{n_i} \mathbf{z}_k^{(i)} \tag{4}$$

$$\mathbf{m} = \sum_{i=1}^{M} P_i \mathbf{m}_i \tag{5}$$

Putting formulas (2)-(3) into (1), we get:

$$\begin{aligned} J_d(\mathbf{z}) =& \sum_{i=1}^{M} P_i [\frac{1}{n_i}\sum_{k=1}^{n_i}(\mathbf{z}_k^{(i)} - \mathbf{m}_i)^T(\mathbf{z}_k^{(i)} - \mathbf{m}_i) \\ &+ (\mathbf{m}_i - \mathbf{m})^T(\mathbf{m}_i - \mathbf{m})] \\ =& \sum_{i=1}^{M} P_i [\frac{1}{n_i}\sum_{k=1}^{n_i}(\mathbf{z}_k^{(i)} - \mathbf{m}_i)^T(\mathbf{z}_k^{(i)} - \mathbf{m}_i)] \\ &+ \sum_{i=1}^{M} P_i [(\mathbf{m}_i - \mathbf{m})^T(\mathbf{m}_i - \mathbf{m})] \\ =& d_{intra} + d_{inter} \end{aligned} \tag{6}$$

where d_{intra} and d_{inter} are the intra-class (within-class) distance and the inter-class (between-class) distance respectively, as shown in Fig. 3 (b). The value of d_{intra} represents the scatter of samples around their respective class-expected vectors. The smaller is, the better is the separability. Whereas the d_{inter} measures the difference between two classes, the larger the value of , the better the separability. Therefore, the ratio value of the d_{inter} to the d_{intra} is used as the separability criterion to evaluate the two impedance feature sets (one captured by BIAM, the other by EIT) [20].

$$J_1 = \frac{d_{inter}}{d_{intra}} \tag{7}$$

To achieve a better separability for the measured bio-impedance, the value of J_1 should be larger. Fig. 3 (c) shows

an example in which Impedance Feature Set 1 has better separability than Impedance Feature Set 2 even with a similar intra-class distance.

III. System design

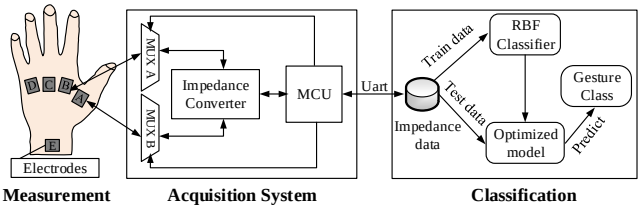

Fig. 4. The overall structure of BIAM system for gesture recognition.

Fig. 4 shows the overall structure of the BIAM gesture recognition system, which consists of three parts: measurement scheme, impedance data acquisition, data processing and algorithm for gesture classification. First, the dimensions of the bio-impedance feature are determined by a measurement scheme. Then, a customized measurement scheme is selected to capture bio-impedance information according to the position and number of electrodes. Next, the impedance data are obtained by a customized BIAM acquisition system, which is composed of two multiplexer (MUX) modules, a microcontroller (MCU) and an impedance converter module, and transmitted to the computer via a universal asynchronous receiver transmitter (Uart) communication for gesture recognition by using a classical classification algorithm SVM with radial basis function (RBF) as a kernel.

A. Measurement Scheme

Two schemes are commonly used for bio-impedance measurement (BIM), one is a two-terminal system, and the other is a four-terminal system.Each system has its own strengths and weaknesses. The four-terminal scheme system employs four electrodes for measurement, one pair of electrodes is used for current injection and another pair of electrodes is used for voltage measurement. The impedance obtained by this method can eliminate the effect of the contact impedance to obtain the internal impedance of the body. However, this method requires two pairs of electrodes for one measurement, which makes the hardware system more sophisticated. In the two-terminal scheme system, only two electrodes were used to carry out current injection and voltage measurements. Owing to its simplicity, it has been widely used in bioimpedance measurements [13], [17], [22]. The disadvantage lies in that the measured impedance includes both contact and body impedances. In this study, we are more interested in detecting the impedance changes for hand gesture recognition, therefore, the two-terminal scheme based on 4-wire bio-impedance measurements(BIM) method [23], is selected, which could remedy the contact impedance while maintaining a simpler system.Fig. 5 shows a schematic diagram of a four-wire BIM system, a precision ac voltage source (AC), a high precision current meter (I_M) and a precision differential voltage meter (V_M) are required [23] for consisting of an impedance converter which converts the measured current and voltage into impedance. We can acquire an accurate injection current I that flows from the contact impedance and body impedance. Compared with the traditional constant current source, this method can achieve a more accurate current injection.V_M has a very high input impedance, so ideally no current flows through it. The voltage measured by the V_M is the voltage across the interior impedance of the human body and the contact impedance.According to the AD5940 manual [23], the impedance was calculated using the following equation:

$$|Z| = \frac{V_{Z_{unknown}}}{I} \tag{8}$$

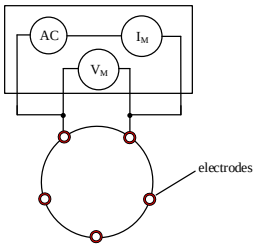

Fig. 5. Two-terminal scheme based on 4-wire bio-impedance measurements with five electrodes.

B. Bio-impedance data acquisition

We designed a customized bio-impedance data acquisition circuit (see Fig. 6) based on AD5940, which is a high-precision, ultra-low power, analog front-end system designed for impedance measurement [23]. This chip implements a 12-bit high speed digital-to-analog converter (DAC) that can generate an AC excitation signal from DC to 200kHz and a 16-bit, 800 kSPS, multichannel successive approximation register (SAR) analog-to-digital converter ADC which can measure high bandwidth signals up to 200 kHz. A constant excitation signal of 40 kHz was used in this study, which was free of ambient noise and was capable of achieving a better recognition of different gestures [13]. Additionally, a digital filtering method was used to improve the signal-to-noise performance as well as the overall measurement accuracy. As such, the sinc filter enabled the 50 Hz or 60 Hz notch filter to filter mains noise. Considering the probable false motion due to the eventual mechanical inertia and/or electrical hysteresis, the average filtering method was applied to preprocess data where ADC results were averaged to trade-off conversion speed against noise signals.

The system architecture of the data acquisition board is showed in Fig. 7. It mainly consists of four parts: current injection, current measurement, voltage measurement and a microcontroller (MCU). The first three parts constitute the impedance converter of our data acquisition system. The waveform generator used with the high-speed DAC generates a given voltage and frequency AC excitation signal as the current injection. A high-power transimpedance amplifier (TIA) converts current flowing through the body impedance and contact impedance into voltage, which can be measured by an analog-to-digital converter (ADC). A high power TIA, an ADC, forms

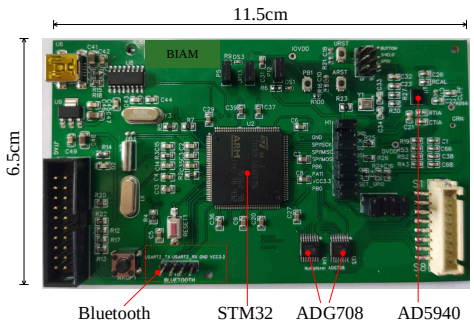

Fig. 6. BIMA data acquisition board.

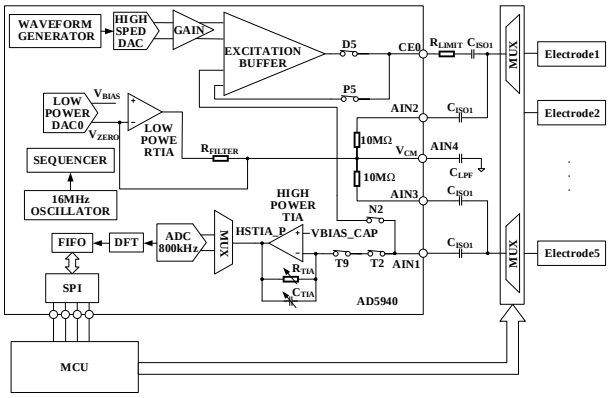

Fig. 7. System architecture of data acquisition board.

current measurement module. A low-power DAC and a low-power TIA comprise a precision differential voltage meter for voltage measurement. Then a discrete Fourier transform (DFT) is performed on the current data and voltage data to calculate their real and imaginary parts. The processed data is sent to MCU to calculate the unknown impedance of the human body via the serial peripheral interface (SPI). Our device is used for body impedance measurement which should conform to the IEC 60601 standard to guarantee safety. The maximum allowable ac current at is 400 μA at 40 kHz and is 500 μA at 50 kHz. To limit the amount of AC current flowing through the human body, a 1 kΩ RLIMIT was selected. According to IEC 60601 standards, the maximum DC current entering the human body cannot exceed 10 μA. In our device, we used four isolation capacitors to ensure that the DC current flowing into the human body was zero. Considering safety and wearable, a value of 0.47 μF is selected for the isolation capacitors. Two 8-to-1 multiplexers ADG708 connect the current injection terminal and current measurement terminal to any two electrodes, making up the signal-projection pair. The voltage measurement terminals are also connected to the same two electrodes by the multiplexers mentioned above, forming a voltage-measuring pair. In other words, the voltage measurement pair was the same as that of the signal projection pair. In practical applications, to minimize the impact of contact impedance, it is necessary to ensure that the contact impedance between the electrodes and skin is small. Furthermore, the contact impedance change should also be small when making gestures, which requires that electrodes should always be in close contact with the skin. In this study, we focused on comparing the recognition results of the two methods. To obtain effective and stable impedance data, we selected medical electrodes with stable performance, which greatly compromised the comfort of wearing. As for the size of the electrode on the impedance acquisition, we did not investigate its effects. Readers who are interested in the electrode effect on the measurement data can refer to [15], in which the authors compared gesture recognition rates by using a series of electrodes with different materials and shapes. Theoretically, the size of the electrode can be reduced to the maximum possible extent. In practice, this study has certain limitations. The commercial medical electrodes we chose were composed of an Ag/AgCl electrode surrounded by a conductive gel. The details of the structure of the medical electrode are shown in Fig. 8 .The gel is surrounded by an adhesive material, which is used to fix the electrodes. Therefore, the use of medical electrodes can also avoid electrode loosening during exercise, making the measurement results more stable.

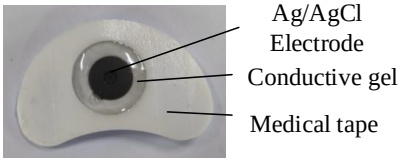

Fig. 8. The structure of medical electrode.

To verify the robustness of the system, an experiment for measuring the voltage signal without excitation was performed, and we found that the voltage amplitude of the measured signal was almost zero during the hand movement. Specifically, we collected 780 samples of voltage amplitude signals that were measured during hand movement with 400 mv excitation and no excitation, respectively. As shown in Fig. 9, we found that the average voltage amplitude was almost zero (0.007 mV) when no excitation signal was applied during hand movement, while the average voltage amplitude was 116.385 mv when 400 mv excitation was applied. This means that when no excitation is applied, the noise caused by hand movement is negligible.

The impedances between all electrode pairs were measured sequentially without repetition, which resulted in 10 independent values (with five electrodes). To accelerate the process of subsequent data analysis, we added an identification termination symbol after each scan, which provides a guarantee for us to carry out real-time continuous measurements. The system achieved a 200 Hz output data rate (ODR) (20 frames per second), which was sufficiently fast for real-time interaction. The generated impedance data were sent to computer for further processing and classification.

C. Data processing and algorithm for gesture classification

In our previous work, impedance data of 28 feature dimensions were collected and feature selection approaches were used to reduce the dimensionality of the data [17]. In

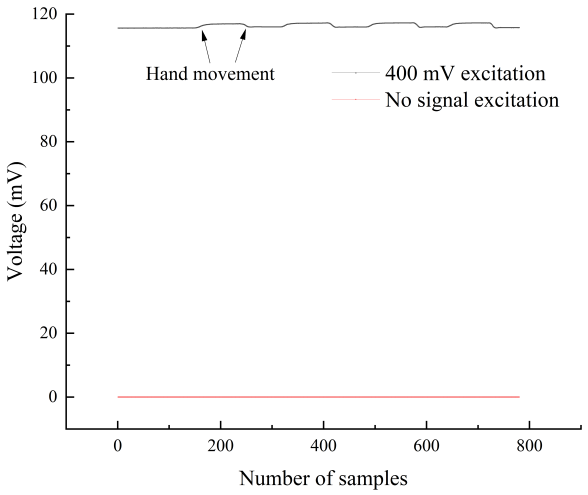

Fig. 9. Comparison of measured voltage signals with and without excitation.

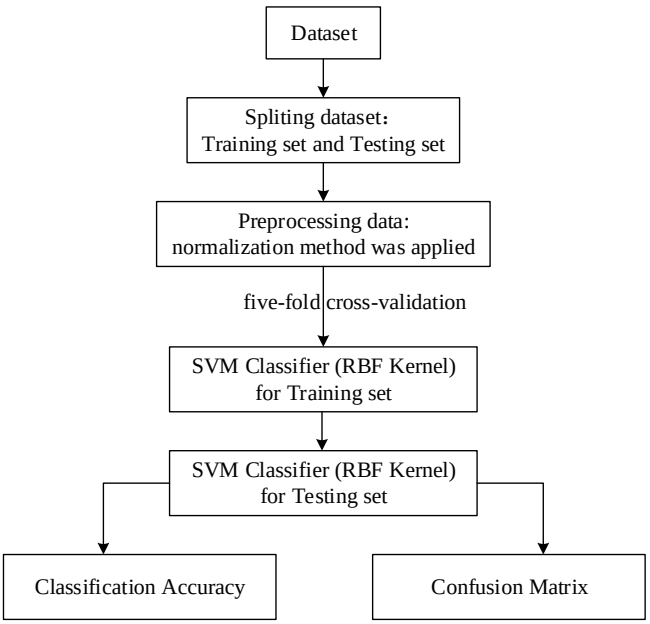

Fig. 10. Software flowchart of the system for gesture recognition.

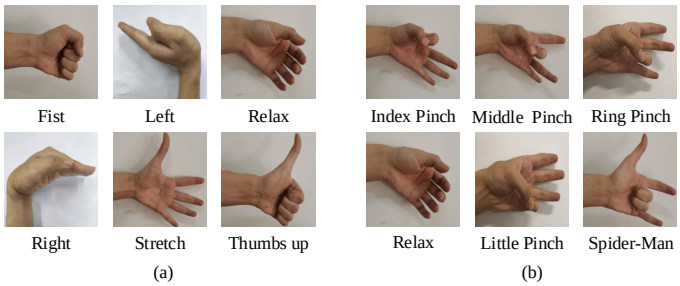

Fig. 11. Hand gestures used in tests; (a) hand gesture set (b) pinch gesture set.

this study, we adopted a two-terminal scheme based on 4-wire measurement method with five electrodes to process the impedance analysis. Ten feature dimensions generated by this method. These ten features are obtained based on the prior information of human anatomy; therefore, no feature selection is required. Fig.10 shows the software flowchart of the system. When collecting the impedance data, digital filtering and average filtering methods were applied to preprocess the data to reduce ambient noise. Additionally, the normalization method was applied to preprocess these data to reduce the effect of the difference due to various users and simultaneously remove the effect of the contact impedance at the same time. Then, a five-fold cross-validation was adapted to the datasets, which were collected within five cycles. We used a support vector machine (SVM) provided by the scikit-learn toolkit for classification [24]. Because SVM is a classic classification algorithm, it can use the kernel function to increase the ability of feature abstraction, and it is suitable for small-scale datasets. According to our previous study [17], we found that the SVM method can achieve a performance trade-off recognition between accuracy and training time. The radial basis function (RBF) was used as the kernel for classification. Finally, we calculated the classification accuracy of the training model on the test set and obtained a confusion matrix.

IV. Results and Discussion

A. Gesture sets

We selected 11 hand gestures mentioned in previous work [13], [17] for comparison. These gestures are divided into two gesture sets (Fig.11). One is a hand gesture set including Fist, Left, Right, Stretch, Thumbs up, which focuses on rough hand gestures. The other is a pinch gesture set including Index Pinch, Little Pinch, Middle Pinch, Ring Pinch, Spider-Man, which focuses on fine hand gestures. The gesture Relax is used in both sets as the neutral state.

The BIAM system is sensitive to the position of the electrode; therefore, we proposed a gesture recognition method that is based on the anatomy of the human hand. In the experimental study, we found that when electrodes are placed in certain positions, small movements of the muscles can be captured, thereby improving the accuracy of gesture recognition. Considering that the system presented in this paper is sensitive to placement, we try our best to ensure that the electrodes are placed in the same position according to the human hand structure during each measurement. We also recruited different people and performed several repeated experiments to reduce the effect of the sensitivity of the system to electrode placement. In this study, five participants (three men and, two women) with a mean age of 25 years were recruited to collect gesture datasets. After a brief introduction, all participants could place the electrodes correctly and the system worked normally. This might be attributed to the fact that we used a small number of electrodes and the selected electrode positions correspond to the anatomical positions of the hand. First, we cleaned the area where the electrodes were placed with medical alcohol. Five electrodes were attached to the designated position. Next, the participants familiarized

themselves with all 11 gestures before testing. To collect impedance data, we designed a customized upper-computer software with Python, which could greatly save time for data collection. For each gesture, we collected 30 test samples in one cycle. Five repeated cycles were performed for each participant. One of the cycles was used as the testing set, and the other four were used as training sets. In total, 18000 samples (five participants×30 samples for one cycle ×five cycles × six gestures (one gesture set) × two gesture sets × two sensor positions) were acquired for the entire experiment. It took approximately 10 min to register the gesture data of two gesture sets for each participant.

B. Impedance measurement and analysis

In BIAM gesture recognition, four electrodes are attached to the dorsum of the hand and one electrode is attached to the palm side of the wrist (Fig. 12 (a)), which is marked as Hand Location. In fact, we placed the electrode "E" at the palm side of the wrist instead of the dorsal wrist. This was because the palmaris longus tendon, the tendons of the flexor digitorum superficialis and profundus are distributed near the skin on the palm side of the wrist, which are directly related to gestures. The Wrist Location where five electrodes were evenly attached to the wrist (Fig. 12 (b)), which is commonly used in EIT recognition applications. We compared the typical impedance

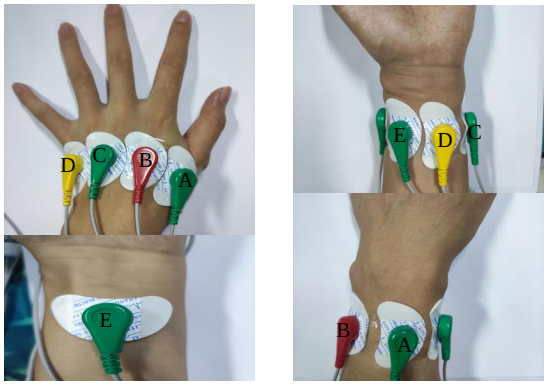

(a) (b)

Fig. 12. Two kinds of electrode positions (a) dorsum of hand and palm side of wrist (Hand Location) (b) wrist (Wrist Location).

values of the two electrode positions on the two gesture sets, as shown in Fig.13 and 14. The gesture impedance value adopted the average value of the collected samples for each gesture. We can clearly observe that the impedance difference between the different gestures when the electrodes are placed at Hand Location is greater than when placed at the wrist. We further calculated the difference between the maximum and minimum impedance values for each of the 10 electrode pairs (AB,AC,...,DE), and the average impedance difference on 10 electrode pairs according to the impedance values shown in Fig. 13 and 14. The results are shown in TABLE I. By comparing the average value of the impedance range, we can roughly find that the BIAM method (Hand Location) has a larger impedance range than the EIT method (Wrist Location),

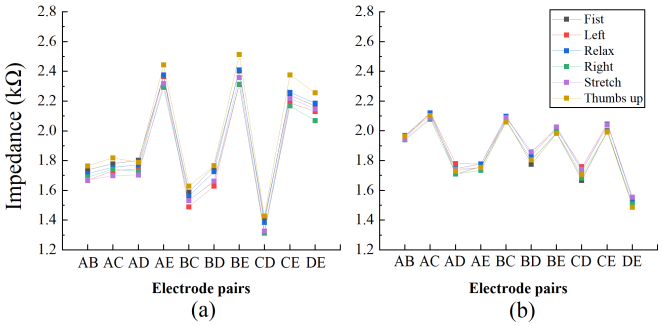

Fig. 13. The impedance data of Hand gesture sets. (a) Hand Location (b)Wrist Location.

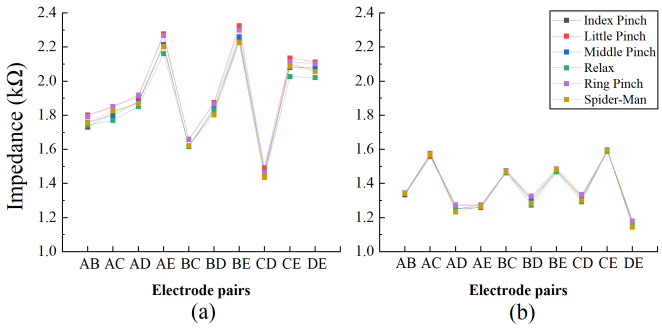

Fig. 14. The impedance data of Pinch gesture sets. (a) Hand Location (b)Wrist Location.

TABLE I
THE AVERAGE IMPEDANCE DIFFERENCE VALUE OF TWO IMPEDANCE DATA SETS OBTAINED FROM THE HAND LOCATION AND WRIST LOCATION

	Hand gesture set		**Pinch gesture set**	
Electrodes pairs	Impedance range for Hand Location (kΩ)	Impedance range for Wrist Location (kΩ)	Impedance range for Hand Location (kΩ)	Impedance range for Wrist Location (kΩ)
AB	0.097	0.029	0.071	0.012
AC	0.12	0.044	0.081	0.017
AD	0.101	0.071	0.067	0.041
AE	0.152	0.043	0.116	0.016
BC	0.14	0.038	0.043	0.014
BD	0.137	0.083	0.073	0.052
BE	0.204	0.043	0.099	0.018
CD	0.115	0.093	0.054	0.044
CE	0.207	0.054	0.108	0.011
DE	0.187	0.068	0.09	0.037
Average	0.146	0.056	0.08	0.026

which also means that the BIAM method will increase the impedance feature difference between gestures.

According to equation (7), we calculated the average separability criterion J_1 of five participants of two gesture sets by two electrode positions, as shown in TABLE II and, when the electrodes were placed at Hand Location, we obtained larger J_1 values for all the gesture sets. This means that the placement of electrodes on the hand increases the inter-class distance between gestures compared to the electrode position at the wrist. Additionally, for both placements, J_1 on the hand gesture set was greater than that on the pinch gesture set. The larger value of the separability criterion J_1 demonstrates that the impedance features of BIAM (captured from Hand Location) can be easily be distinguished from those of EIT (captured from Wrist Location), which is more salient for hand gesture recognition.

TABLE II
THE AVERAGE SEPARABILITY CRITERION VALUE OF TWO IMPEDANCE DATA SETS OBTAINED FROM THE HAND LOCATION AND WRIST LOCATION FOR FIVE USERS

Gesture sets	Electrode Location	J_d
Hand gesture set	Hand Location	0.252
	Wrist Location	0.149
Pinch gesture set	Hand Location	0.233
	Wrist Location	0.118

C. Accuracy

Considering that different users have various bio-body conditions, we used the per-user classifiers mentioned in [14] to process the measurement data separately. The support vector machine (SVM) provided by the scikit-learn toolkit was applied for classification [24] in this study. The recognition accuracy was estimated using a five-fold cross-validation method using 3600 datasets for each user. Specifically, we trained the classifier on four rounds of a user's data, and tested it on the fifth (all combinations) and the accuracy was calculated as the ratio of the number of gestures correctly classified to the total dataset for testing. We evaluated the final accuracy by averaging the results per user. The accuracy of the hand gesture set and pinch gesture set for two electrode positions (Hand Location and Wrist Location) are shown in Fig.15. For the hand gesture set, the Wrist Location achieved an accuracy of 97.1%, while the Hand Location achieved an accuracy of 98.7%; however, for the pinch gesture set, the electrodes arranged on the Hand Location obtained much better results with a recognition accuracy of 97.8% in comparison with 86.3% for the Wrist Location.

Fig. 16 (a, b) shows confusion matrices of the hand gesture set for Wrist Location and Hand Location, respectively. The rows of the matrix represent instances of the actual class (i.e. an actual gesture), and the columns of the matrix represent instances of the predicted class (i.e. the predicted gesture). In the confusion matrix, the values of the diagonal elements represent the percentages of correctly predicted classes. The mistakenly confusion with other classes is expressed by falsely

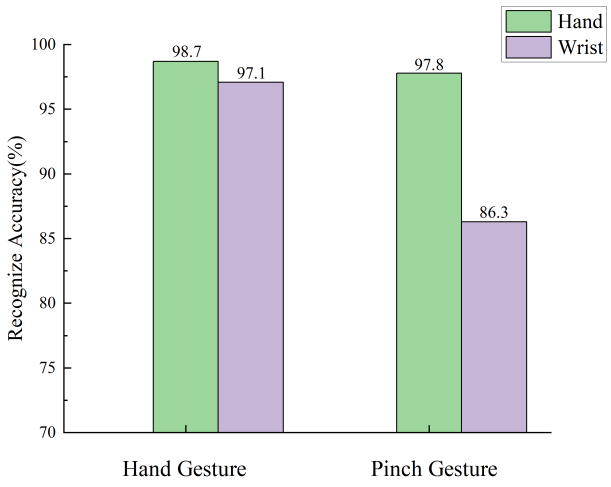

Fig. 15. Accuracy of hand gesture set and pinch gesture set for electrodes arranged on two positions: Hand Location and Wrist Location.

classified off-diagonal elements. The sum of each row is 100%. Fig.16 (a) shows that Fist has the lowest predicted accuracy of 94.4% due to the confusion with Relex, Right and Thumbs up, while it increases to 96.8% in the Hand Location as shown in Fig. 16 (b). These results might be attributed to the fact that Fist, Relax, Right, and Thumbs up have similar muscle contractions that cannot be easily distinguished by the EIT method which wrapped electrodes around the wrist. However, for the BIAM method in which the electrodes were placed on the hand location, these gestures were less likely to be confused because of the obtained impedance difference among the gestures using the electrodes at the Hand Location is greater than that at the Wrist Location.

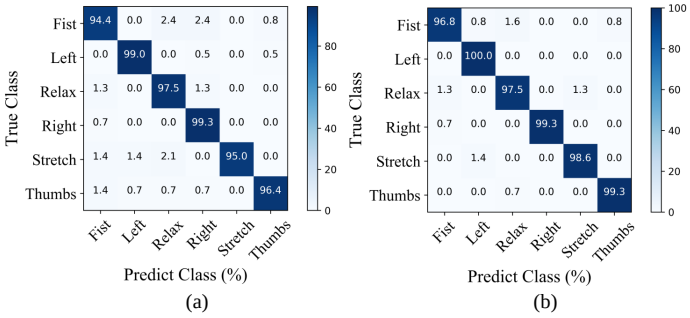

Fig. 16. Confusion matrix across hand gesture sets using SVM classifier.(a) Wrist Location (b) Hand Location.

For the pinch gesture set, Wrist Location achieved a poor mean accuracy of 86.3%, while the Hand Location achieved a mean accuracy of 97.8%. Fig.17 (a) shows that Ring pinch has the lowest predicted accuracy of 80.7% by the EIT method which is most likely confused with Little pinch; however, the predicted accuracy increased to 92.9% by the BIAM method with electrodes placed on the Hand Location as shown in Fig.17 (b). This is because the impedance signals of Little pinch and Ring pinch are very similar that can not be easily discriminated (Fig. 14 (b)). Zhang and Harrison [13] found the

similar phenomenon of that Ring Pinch and Little Pinch can be mostly confused with each other by the EIT method which used eight electrodes wrapped around the wrist. Although more electrodes were used to measure the impedance signals, they still only got an average accuracy of 86.5% for five pinch gestures. However, the proposed BIAM method based on human hand anatomy can detect the minimum change in bio-impedance of the human body corresponding to the hand movement, consequently improving the gesture recognition accuracy.

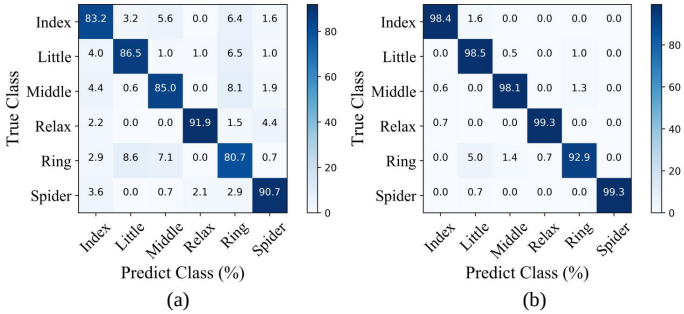

Fig. 17. Confusion matrix across Pinch gesture sets using SVM classifier.(a) Wrist Location (b) Hand Location.

By comparing the above experimental results, we found that: 1) The accuracy of gesture recognition on the pinch gesture set was generally lower than that on the hand gesture set. Because gestures in the pinch set employed similar muscle movements, which caused the impedance difference between the gestures to be small, they were more difficult to distinguish from each other compared to hand gestures. 2) The electrodes position had a significant influence on the accuracy of gesture recognition. The accuracy of gesture recognition at Hand Location was significantly higher than that of Wrist Location, indicating that Hand Location were easier to capture signal changes in hand movements. 3) The results presented in TABLE II and Fig.15 clearly demonstrate that the greater the impedance difference, the higher the accuracy of gesture recognition. It also verified our idea that optimizing the electrode position to obtain larger impedance difference is a way to improve the accuracy of gesture recognition.

D. Real-time gesture recognition

We compared the real-time performance of BIAM-based (electrodes placed on the Hand location) and EIT-based (electrodes wrapped around Wrist location) hand gesture recognition on the two gesture sets separately. A part of the recognition results is shown in Fig. 18. When we make a gesture, the BIAM system obtains the impedance data and sends it to the laptop. The recognition result are displayed in the form of gesture pictures. The experimental results indicate that the proposed BIAM (Hand Location) can improve the accuracy of gesture recognition (S video I and video II).

V. CONCLUSION AND FUTURE WORK

We proposed a BIAM-based gesture recognition system by choosing the electrode positions in accordance with the

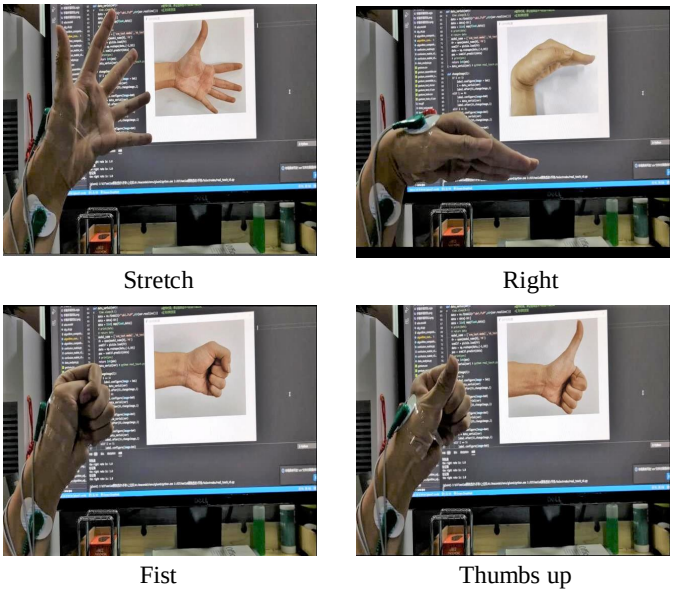

Fig. 18. Real-time gesture recognition with optimal electrode position.

structure of the human hand,which demonstrated the advantage of distinguishing gestures with similar muscle contractions on the wrist. By detecting the minimum change of bio-impedance signals corresponding to the hand movement, we can achieve a high classification accuracy in hand gesture recognition with flexibility in electrode arrangement and fewer electrodes in comparison with the EIT method, which placed electrodes around the hand wrist. This method can achieve an accuracy of 98.7% for the hand gesture set and 97.8% for the pinch gesture set with five electrodes for 11 gestures. It is also convenient to add more electrodes to recognize more than eleven gestures. Currently, we can only realize static gesture recognition. In the future, we will further explore the relationship between gestures and impedance values to achieve dynamic gesture recognition. The BIAM method has the advantages of high gesture recognition accuracy, feasibility and wearability. However, this study is still in the early stages of research and is far from practical application. For practical utilization of the system, more work should be performed to improve the electrode system for bio-impedance measurements with wearability, comfortability and durability.

REFERENCES

[1] Y. Wu, D. Jiang, J. Duan, X. Liu, R. Bayford, and A. Demosthenous, "Towards a high accuracy wearable hand gesture recognition system using eit," in *2018 IEEE International Symposium on Circuits and Systems (ISCAS)*. IEEE, 2018, pp. 1–4.

[2] Z. Ren, J. Yuan, J. Meng, and Z. Zhang, "Robust part-based hand gesture recognition using kinect sensor," *IEEE transactions on multimedia*, vol. 15, no. 5, pp. 1110–1120, 2013.

[3] G. Plouffe and A.-M. Cretu, "Static and dynamic hand gesture recognition in depth data using dynamic time warping," *IEEE transactions on instrumentation and measurement*, vol. 65, no. 2, pp. 305–316, 2015.

[4] O. K. Oyedotun and A. Khashman, "Deep learning in vision-based static hand gesture recognition," *Neural Computing and Applications*, vol. 28, no. 12, pp. 3941–3951, 2017.

[5] A. Dementyev and J. A. Paradiso, "Wristflex: low-power gesture input with wrist-worn pressure sensors," in *Proceedings of the 27th annual ACM symposium on User interface software and technology*. Association for Computing Machinery, 2014, pp. 161–166.

[6] Y. Xia, H. Heidari, and R. Ghannam, "Smart wristband for gesture recognition," in *2020 International Conference on UK-China Emerging Technologies (UCET)*. IEEE, 2020, pp. 1–4.

[7] P.-G. Jung, G. Lim, S. Kim, and K. Kong, "A wearable gesture recognition device for detecting muscular activities based on air-pressure sensors," *IEEE Transactions on Industrial Informatics*, vol. 11, no. 2, pp. 485–494, 2015.

[8] R. Xu, S. Zhou, and W. J. Li, "Mems accelerometer based nonspecific-user hand gesture recognition," *IEEE sensors journal*, vol. 12, no. 5, pp. 1166–1173, 2011.

[9] H. P. Gupta, H. S. Chudgar, S. Mukherjee, T. Dutta, and K. Sharma, "A continuous hand gestures recognition technique for human-machine interaction using accelerometer and gyroscope sensors," *IEEE Sensors Journal*, vol. 16, no. 16, pp. 6425–6432, 2016.

[10] D. Farina, J. Ning, H. Rehbaum, A. Holobar, B. Graimann, H. Dietl, and O. C. Aszmann, "The extraction of neural information from the surface emg for the control of upper-limb prostheses: Emerging avenues and challenges," *IEEE Transactions on Neural Systems and Rehabilitation Engineering*, vol. 22, no. 4, pp. 797–809, 2014.

[11] X. Chen, Y. Li, R. Hu, X. Zhang, and X. Chen, "Hand gesture recognition based on surface electromyography using convolutional neural network with transfer learning method," *IEEE Journal of Biomedical and Health Informatics*, pp. 1–1, 2020.

[12] W. Geng, Y. Du, W. Jin, W. Wei, Y. Hu, and J. Li, "Gesture recognition by instantaneous surface emg images," *scientific reports*, vol. 6, no. 1, pp. 36 571–36 571, 2016.

[13] Y. Zhang and C. Harrison, "Tomo: Wearable, low-cost electrical impedance tomography for hand gesture recognition," in *Proceedings of the 28th Annual ACM Symposium on User Interface Software & Technology*. ACM, 2015, pp. 167–173.

[14] Y. Zhang, R. Xiao, and C. Harrison, "Advancing hand gesture recognition with high resolution electrical impedance tomography," in *Proceedings of the 29th Annual Symposium on User Interface Software and Technology*. ACM, 2016, pp. 843–850.

[15] J. Yao, H. Chen, Z. Xu, J. Huang, J. Li, J. Jia, and H. Wu, "Development of a wearable electrical impedance tomographic sensor for gesture recognition with machine learning," *IEEE Journal of Biomedical and Health Informatics*, vol. 24, no. 6, pp. 1550–1556, 2019.

[16] D. Jiang, Y. Wu, and A. Demosthenous, "Hand gesture recognition using three-dimensional electrical impedance tomography," *IEEE Transactions on Circuits and Systems II: Express Briefs*, vol. 67, no. 9, pp. 1554–1558, 2020.

[17] G. Ma, Z. Hao, X. Wu, and X. Wang, "An optimal electrical impedance tomography drive pattern for human-computer interaction applications," *IEEE Transactions on Biomedical Circuits and Systems*, vol. 14, no. 3, pp. 402–411, 2020.

[18] N. Hyvonen, A. Seppänen, and S. Staboulis, "Optimizing electrode positions in electrical impedance tomography," *SIAM Journal on Applied Mathematics*, vol. 74, no. 6, pp. 1831–1851, 2014.

[19] D. Smyl and D. Liu, "Optimizing electrode positions in 2-d electrical impedance tomography using deep learning," *IEEE Transactions on Instrumentation and Measurement*, vol. 69, no. 9, pp. 6030–6044, 2020.

[20] A. R. Webb, *Statistical pattern recognition*. John Wiley & Sons, 2003.

[21] K. L. Moore and A. F. Dalley, *Clinically oriented anatomy*. Wolters kluwer india Pvt Ltd, 2018.

[22] J. Chen, L. Xu, Z. Cao, and H. Zhou, "Four-terminal imaging using a two-terminal electrical impedance tomography system," *IEEE Transactions on Instrumentation and Measurement*, vol. 63, no. 2, pp. 432–440, 2013.

[23] A. Devices, "High precision, impedance, and electrochemical front end ad5940/5941," Data Sheet. [Online]. Available: https://www.analog.com/media/en/technical-documentation/data-sheets/AD5940-5941.pdf

[24] F. Pedregosa, G. Varoquaux, A. Gramfort, V. Michel, B. Thirion, O. Grisel, M. Blondel, P. Prettenhofer, R. Weiss, V. Dubourg, J. Vanderplas, A. Passos, D. Cournapeau, M. Brucher, M. Perrot, and E. Duchesnay, "Scikit-learn: Machine learning in Python," *Journal of Machine Learning Research*, vol. 12, pp. 2825–2830, 2011.

Haofeng Chen (陈皓枫) received the B.S. degree in mechanical design, manufacture and automation from Xidian University, Xi'an, China, in 2018. He is currently working toward the Ph.D. degree with the Hefei Institutes of Physical Science, Chinese Academy of Sciences, Hefei, China, and doing research on EIT based tactile sensors at the Bioinspired Robotics and Intelligent Material Laboratory, Institute of Advanced Manufacturing Technology, Chinese Academy of Sciences. His research interests include biomedical image/signal processing, electrical impedance tomography, machine learning and tactile sensing.

Gang Ma (马刚) received the B.S. degree in electrical engineering from Zhengzhou University, Zhengzhou, China, in 2015, the Ph.D. degree from the Department of Precision Machinery and Precision Instrumentation, University of Science and Technology of China, Hefei, China, in 2021. His research interests include biomedical image/signal processing, electrical impedance tomography and machine learning.

Peng Wang (王鹏) received the master degree in the School of Automation from Chongqing University of Posts and Telecommunications, Chongqing, China, in 2021. He is currently working as an algorithm engineer in Shenzhen Apulis Technology Inc. His research interests include deep learning, electrical impedance tomography(EIT) and computer vision.

Xiaojie Wang (王晓杰) received the B.S. degree in fluid mechanics from Tsinghua University, Beijing, China, in 1989, the M.S. degree in solid mechanics from the University of Science and Technology of China, Hefei, China, in 1998, and the Ph.D. degree from the Department of Mechanical Engineering, University of Nevada, Reno, NV, USA, in 2002.

Dr. Wang is the Founder and Director of the Bio-inspired Robotics and Intelligent Material Laboratory, Institute of Advanced Manufacturing Technology, Chinese Academy of Sciences, Beijing, China. He is an Adjunct Professor with the University of Science and Technology of China, Hefei, China, and also serves as External Supervisor in the Faculty of Engineering and Information Technology, University of Technology Sydney, Australia. Prior to joining the CAS, he had been conducting research on intelligent materials and devices at University of Nevada, Reno for more than 10 years. He is author/coauthor of more than 150 scientific publications with chapters in three books and holds six patents. His research interests are in the areas of bio-inspired robots, smart materials, sensor/actuator and mechatronic systems.